Acta Crystallographica Section D
Biological Crystallography
ISSN 0907-4449

C3 exoenzyme from *Clostridium botulinum*: structure of a tetragonal crystal form and a reassessment of NAD-induced flexure

Hazel R. Evans,[a] Daniel E. Holloway,[a] J. Mark Sutton,[b] Joanne Ayriss,[b] Clifford C. Shone[b] and K. Ravi Acharya[a]*

[a]Department of Biology and Biochemistry, University of Bath, Claverton Down, Bath BA2 7AY, England, and [b]Health Protection Agency, Centre for Applied Microbiology and Research, Porton Down, Salisbury SP4 OJG, England

Correspondence e-mail: k.r.acharya@bath.ac.uk

Received 15 March 2004
Accepted 12 May 2004

PDB Reference: C3 exoenzyme, tetragonal form, 1uzi, r1uzisf.

C3 exoenzyme from *Clostridium botulinum* (C3bot1) ADP-ribosylates and thereby inactivates Rho A, B and C GTPases in mammalian cells. The structure of a tetragonal crystal form has been determined by molecular replacement and refined to 1.89 Å resolution. It is very similar to the apo structures determined previously from two different monoclinic crystal forms. An objective reassessment of available apo and nucleotide-bound C3bot1 structures indicates that, contrary to a previous report, the protein possesses a rigid core formed largely of β-strands and that the general flexure that accompanies NAD binding is concentrated in two peripheral lobes. Tetragonal crystals disintegrate in the presence of NAD, most likely because of disruption of essential crystal contacts.

1. Introduction

C3 exoenzyme from *Clostridium botulinum* (Aktories *et al.*, 1987), also known as C3bot1, is the best characterized member of the C3 exoenzyme family, which also includes C3lim from *C. limosum*, C3cer from *Bacillus cereus* and the C3stau/EDIN subfamily from *Staphylococcus aureus* (reviewed by Wilde & Aktories, 2001). These ~24 kDa enzymes specifically ADP-ribosylate and thereby inactivate mammalian Rho GTPases, a group of membrane-associated molecular switches that regulate many cell functions (Bokoch, 2000). C3bot1 specifically modifies Rho A, B and C (Braun *et al.*, 1989; Aktories *et al.*, 1989; Chardin *et al.*, 1989). This process brings about a variety of cellular changes, some of which are morphological: adherent cells 'round up' (Chardin *et al.*, 1989), monocytes spread out (Aepfelbacher *et al.*, 1996) and neuronal PC12 cells exhibit neurite outgrowth (Rubin *et al.*, 1988). C3bot1 also stimulates the regeneration of injured axons *in vivo* (Lehmann *et al.*, 1999), highlighting its potential for the treatment of certain neural disorders (Watanabe *et al.*, 2000). However, the role of C3 exoenzymes in the pathogenesis of bacterial disease is unclear because of the lack of an obvious cell-entry mechanism.

In common with many other bacterial toxins, C3bot1 possesses glycohydrolytic activity that splits NAD into nicotinamide and ADP-ribose, the latter of which is transferred to a specific residue of the target protein. Crystal structures of C3bot1 in the absence and presence of NAD have indicated that the mechanism of ADP-ribosylation is structurally complex, involving localized conformational changes of the ADP-ribosylating turn–turn (ARTT) and phosphate–nicotinamide (PN) loops, plus an independent more widespread protein flexure (Han *et al.*, 2001; Ménétrey *et al.*, 2002). Current structural information has been obtained from two different monoclinic crystal forms, but tetragonal crystals that failed to yield useful data have also been reported (Han *et al.*, 2001). Here, we report the production of improved tetragonal crystals, the determination of their structure and a reassessment of the conformational changes observed in the various C3bot1 structures.

2. Experimental

The *C3bot1* gene was kindly supplied by Dr M. R. Popoff (Institut Pasteur, Paris, France). PCR was used to introduce an *Eco*RI site at each end of the gene and a factor Xa cleavage site immediately upstream of the first residue of the mature protein (Ala41). The forward primer was 5′-G**GAATTC**ATCGAAGGTC-GTGCTTATTCAAATACTTACCAGGAG-3′ and the reverse primer was 5′-G**GAAT-TC**TTATTTAGGATTGATAGCTGTGCC-3′ (*Eco*RI sites in bold). The PCR product was restricted with *Eco*RI, ligated with pBCmalE and expressed in *Escherichia coli* JM109 as an MBP-fusion protein as described for C3stau2 (Evans *et al.*, 2003). The protein bound poorly to amylose affinity resin. Instead, the soluble lysate was passed through an SP-Sepharose column (Amersham Biosciences) equilibrated with 20 m*M* HEPES–NaOH pH 7.3. The protein was then eluted with an ascending NaCl concentration gradient and treated with factor Xa to release the C3bot1. The protein was further purified by cation-exchange and gel-filtration chromatography and then concentrated as described previously for C3stau2 (Evans *et al.*, 2003). The final

preparation was stored at 203 K in 20 m*M* HEPES–NaOH pH 7.3, 20 m*M* NaCl, 5 m*M* $MgCl_2$, 1 m*M* EDTA and was >95% pure as judged by SDS–PAGE.

Single crystals were grown by a modification of the method of Han *et al.* (2001). Hanging drops containing 1.5 µl C3bot1 (35 mg ml^{-1}) and 1.5 µl reservoir solution (18% PEG 3350, 3% saturated Na_3VO_4 solution, 0.15 *M* NaCl and 0.1 *M* imidazole/malate pH 5.5) were incubated at 292 K and produced tetragonal crystals within 2 d. A range of ligand-binding experiments were conducted in which crystals were soaked for 0.5–30 h in reservoir solution supplemented with 9% PEG 3350 and 5–100 m*M* of either NAD, ADP-ribose or nicotinamide. Crystals tolerated nicotinamide but disintegrated within 3 h in the presence of either nucleotide. Intact soaked crystals were transferred briefly to a cryoprotectant composed of reservoir solution supplemented with 9% PEG 3350 and 20% glycerol before collection of diffraction data at 100 K on station PX 9.6 of the SRS, Daresbury, UK.

Crystals soaked in NAD or ADP-ribose diffracted poorly. However, a high-resolution data set was collected from a crystal soaked for 30 h with 100 m*M* nicotinamide. The data were processed and scaled with *HKL*2000 (Otwinowski & Minor, 1997) and reduced with *TRUNCATE* (French & Wilson, 1978); detailed crystallographic statistics are presented in Table 1. Initial phases were determined by molecular replacement with *MOLREP* (Vagin & Teplyakov, 1997) using PDB entry 1g24 molecule *A* (Han *et al.*, 2001) as a search model. Refinement was then carried out with *REFMAC*5 (Murshudov *et al.*, 1997) using NCS restraints for the first few rounds. An initial round of rigid-body refinement was followed by cycles of restrained refinement, electron-density map calculation and model building using *O* (Jones *et al.*, 1991). Atoms for which there was negligible density were not modelled. The $F_o - F_c$ electron-density map showed no evidence of nicotinamide binding, but did indicate the positions of one cyclic tetrametavanadate ion, three orthovanadate ions and two glycerol molecules. Finally, water molecules were added using the *ARP*/*wARP* module

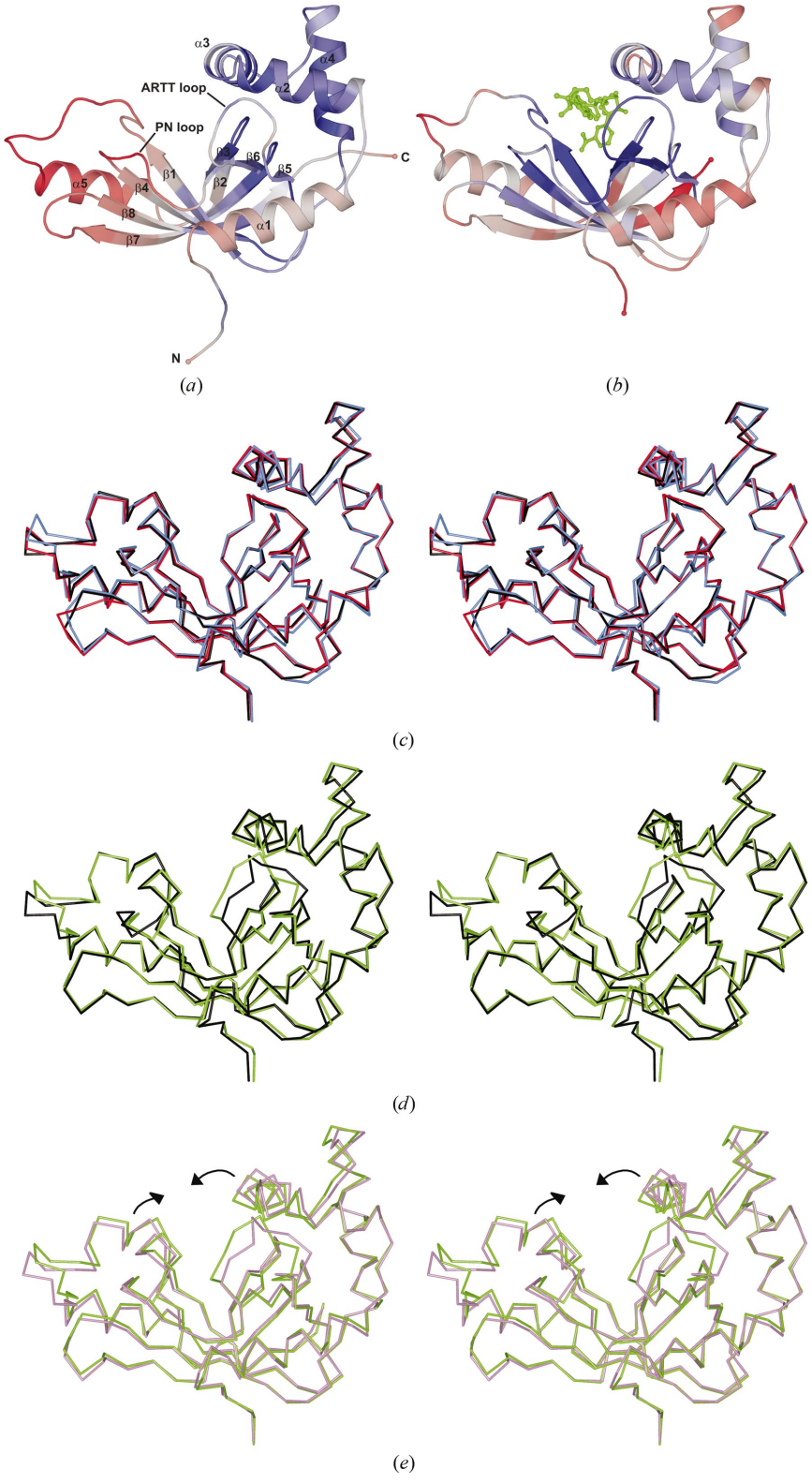

Figure 1
(*a*) Schematic representation of C3bot1 (molecule *A*) from tetragonal crystals. Structural elements are coloured according to C^{α} *B* factor, ranging from 15.0 (blue) to 62.5 Å^2 (red) (mean = 29.3 Å^2). (*b*) C3bot1–NAD complex. Structural elements of PDB entry 1gzf molecule *A* are coloured as in (*a*), ranging from 22.7 (blue) to 77.2 Å^2 (red) (mean = 33.1 Å^2) and the nucleotide is shown in green in a ball-and-stick representation. (*c*) Superposition of the C^{α} traces from three apo C3bot1 structures. Shown in stereo are residues *A*45–*A*246 from tetragonal crystals (black), PDB entry 1g24 (red) and PDB entry 1gze (blue). (*d*) Superposition of the C^{α} traces from apo-C3bot1 and the C3bot1–NAD complex. Shown in stereo are residues *A*45–*A*246 from tetragonal crystals (black) and the C3bot1–NAD complex (PDB entry 1gzf; green). (*e*) Superposition of the C^{α} traces from the C3bot1–NAD and C3bot1–ADP complexes. Shown in stereo are residues 45–246 from the C3bot1–NAD (PDB entry 1gzf, molecule *A*; green) and C3bot1–ADP (PDB entry 1gzf, molecule *D*; purple) complexes. Arrows denote the main-chain flexure that is necessary to convert the ADP-bound to the NAD-bound structure.

(Perrakis *et al.*, 1999) of *REFMAC*5. The stereochemical quality of the structure was checked with *PROCHECK* (Laskowski *et al.*, 1993). Refinement statistics are given in Table 1.

The conformational relationships between the final structure, the apo structures within PDB entries 1g24 (Han *et al.*, 2001) and 1gze (Ménétrey *et al.*, 2002) and the four nucleotide-bound structures comprising PDB entry 1gzf (Ménétrey *et al.*, 2002) were examined with *HINGEFIND* (Wriggers & Schulten, 1997). The program's adaptive selection algorithm was used to identify the principal rigid domain from a common set of residues (45–246). This served as the basis for all structural alignments. Figures were created with *PyMOL* (DeLano Scientific, San Carlos, CA, USA).

3. Results and discussion

3.1. Structure determination

The mosaicity of our best crystal (~0.6°) was significantly less than that of Han *et al.* (2001) (>1.5°). Moreover, the diffraction data it yielded led to a clear molecular-replacement solution. A lack of *h*00 reflections suggested the *I*422 space group described previously, but examination of crystal packing revealed that the correct space group was in fact *I*4. Several factors may have contributed to the improvement in diffraction quality: the different method of protein purification, the reduced precipitant concentration used for crystallization and the stabilization/dehydration of the crystals that occurred during soaking in an elevated precipitant concentration prior to data collection.

Table 1
Crystallographic statistics.

Values in parentheses are for the highest resolution shell (1.96–1.89 Å).

Crystal system	
Space group	*I*4
Unit-cell parameters (Å)	a = 73.3, b = 73.3, c = 218.2
Diffraction data	
Resolution range (Å)	50–1.89
Reflections recorded	683474
Unique reflections	41904
R_{sym}† (%)	9.4 (35.7)
$I/\sigma(I)$	15.3 (4.4)
Reflections with $I > 3\sigma(I)$ (%)	81.8 (53.8)
Completeness (%)	91.6 (91.8)
Final model	
R_{cryst}‡	0.205
R_{free}§	0.253
Deviations from ideality (r.m.s.)	
Bond lengths (Å)	0.019
Bond angles (°)	1.64
Contents of asymmetric unit	
Protein molecules	2
Protein atoms	3195
Water atoms	308
Ligand atoms	43
Mean *B* factor by atom type	
Protein	29.9
Water	33.3
Ligands	52.7

† $R_{sym} = \sum_h \sum_i |I_i(h) - \langle I(h)\rangle| / \sum_h \sum_i I_i(h)$, where $I_i(h)$ and $\langle I(h)\rangle$ are the *i*th and the mean measurements of the intensity of reflection *h*, respectively. ‡ $R_{cryst} = \sum_h |F_o - F_c| / \sum_h F_o$, where F_o and F_c are the observed and calculated structure-factor amplitudes of reflection *h*, respectively. § R_{free} is equal to R_{cryst} for a randomly selected 5% of reflections not used in the refinement (Brünger, 1992).

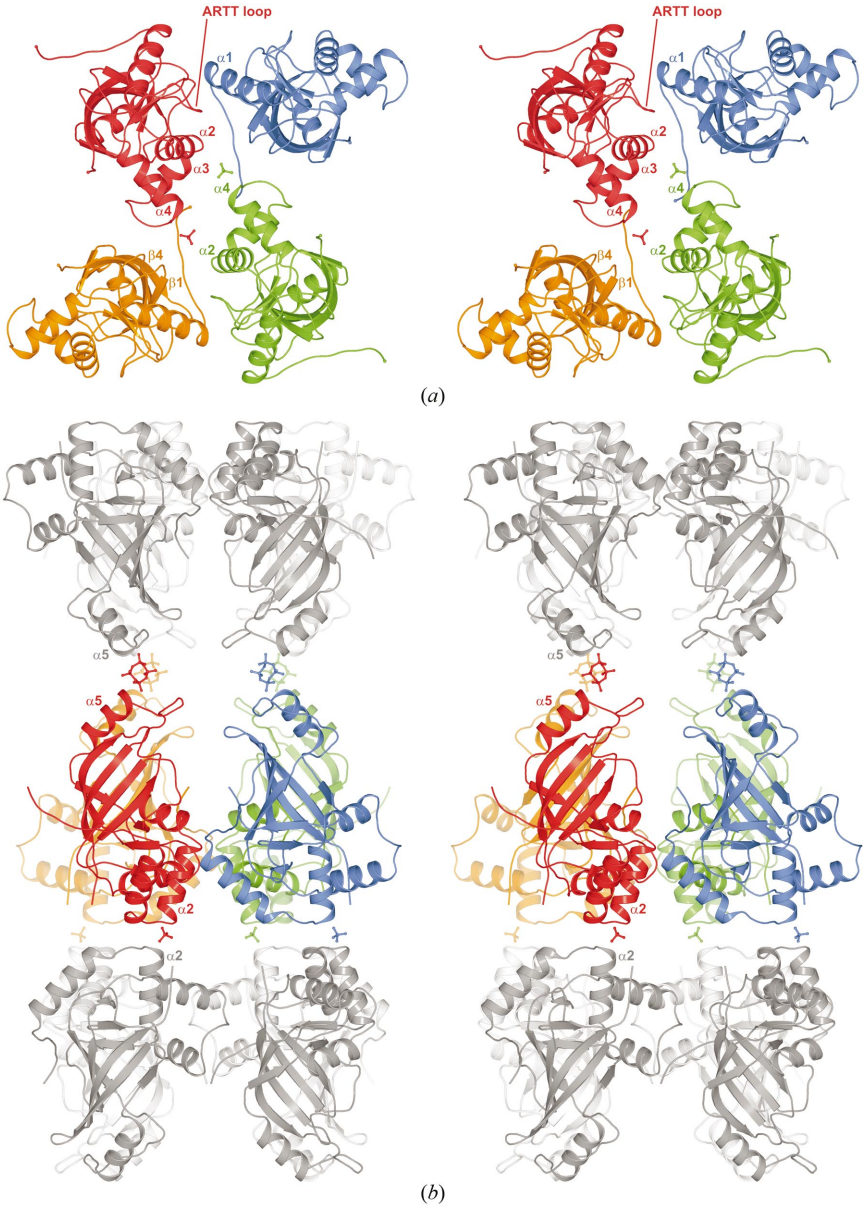

Figure 2
Stereoview of the packing of tetragonal C3bot1 crystals. (*a*) Perpendicular view of a portion of an '*A*' layer. (*b*) In-plane view of the same layer plus adjacent '*B*' layers. Symmetry-related *A* molecules are shown in colour, *B* molecules in grey and secondary-structure elements making crystal-packing contacts are labelled. Cyclic tetrametavanadate and orthovanadate ions are shown in ball-and-stick representation.

3.2. Overall structure

The asymmetric unit contains two C3bot1 molecules. The final model includes every residue (41–251) of each molecule, although the extremities of 23 residues from molecule *A* and 16 from molecule *B* could not be modelled. There are no significant differences between molecules *A* and *B* and their entire C^{α} traces show an r.m.s. deviation of just 0.13 Å. In the Ramachandran plot, 94% of the residues lie in the most favoured region, with only 0.5% (Ala184 from each molecule) in the strongly disfavoured region. This residue is also observed in an unusual conformation in several of the C3bot1 copies present in monoclinic crystals. The general topology is identical to that reported previously (Fig. 1*a*) and the main-

chain trace is remarkably similar to that of PDB entry 1g24 (C^{α} r.m.s. deviation = 0.46 Å), the only notable differences occurring at points in the $\beta1$–$\alpha5$ and $\beta7$–$\beta8$ loops with no obvious functional significance (Fig. 1*c*). It is less similar to PDB entry 1gze, which shows additional localized differences distant from the active site (Fig. 1*c*).

3.3. Conformational flexibility

The distribution of main-chain *B* factors indicates that the lobe that extends outward from the tips of strands $\beta1$, $\beta4$, $\beta7$ and $\beta8$ toward helix $\alpha5$ is a relatively flexible part of the molecule (Fig. 1*a*). Within this lobe, parts of the $\beta1$–$\alpha5$, $\beta3$–$\beta4$ (PN) and $\beta7$–$\beta8$ loops have weak density and are presumed to be particularly flexible. It is of note that the conformational change that accompanies NAD binding significantly increases the relative stability of the lobe (Fig. 1*b*). A search for rigid domains with *HINGEFIND* reveals that the basis and the magnitude of the conformational change are different from those alluded to by Ménétrey *et al.* (2002). It shows that the molecule possesses a rigid core formed largely from the β-strands and that significant main-chain deviations are restricted to peripheral substructures, namely the $\beta5$–$\beta6$ (ARTT) loop, the PN loop and the C-terminal end of the $\beta1$–$\alpha5$ loop (Fig. 1*d*). The magnitude of any widespread main-chain flexure is considerably smaller than that suggested previously.

The two most extreme C3bot1 conformers observed to date are NAD-bound molecule *A* and ADP-bound molecule *D* from PDB entry 1gzf. Following alignment of rigid domains with *HINGEFIND*, a concerted movement of the $\alpha5$ lobe is detectable (Fig. 1*e*), confirming the flexibility suggested by the preceding *B*-factor analysis. In addition, the parts of helices $\alpha2$, $\alpha3$ and $\alpha4$ nearest the nucleotide also move significantly. For each half of the clasping action, the axis of movement is aligned approximately with the viewpoint of Fig. 1. However, φ/ψ angle comparisons suggest that the flexure derives from a large number of small main-chain adjustments rather than rotation about conformational hot-spots.

3.4. Ligand binding and crystal packing

The binding of nicotinamide was too weak to be detected despite an experimental pH that was close to the optima for both the forward and reverse enzyme reactions (Habermann *et al.*, 1991). However, soaking with 5 m*M* NAD or ADP-ribose caused crystal disintegration. This may be because several segments of the protein that move upon NAD binding (Ménétrey *et al.*, 2002) are involved in crystal packing (Fig. 2). The packing gives the crystals a lamellar structure in which '*A*' layers alternate with similarly packed '*B*' layers. The majority of contacts occur within the layers, notable participants being significant portions of the ARTT loop and helices $\alpha3$ and $\alpha4$. The intra-layer contacts are somewhat unusual in that they involve no direct protein–protein interactions but are instead mediated by cyclic tetrametavanadate and orthovanadate ions. These involve helices $\alpha2$ and $\alpha5$, are distant from the nucleotide-binding site, and are likely to have less impact on nucleotide binding.

This work was supported by a postgraduate studentship held jointly between the Health Protection Agency and the University of Bath.

References

Aepfelbacher, M., Essler, M., Huber, E., Czech, A. & Weber, P. C. (1996). *J. Immunol.* **157**, 5070–5075.
Aktories, K., Braun, U., Rösener, S., Just, I. & Hall, A. (1989). *Biochem. Biophys. Res. Commun.* **158**, 209–213.
Aktories, K., Weller, U. & Chhatwal, G. S. (1987). *FEBS Lett.* **212**, 109–113.
Bokoch, G. M. (2000). *Immunol. Res.* **21**, 139–148.
Braun, U., Habermann, B., Just, I., Aktories, K. & Vandekerckhove, J. (1989). *FEBS Lett.* **243**, 70–76.
Brünger, A. T. (1992). *Nature (London)*, **355**, 472–474.
Chardin, P., Boquet, P., Madaule, P., Popoff, M. R., Rubin, E. J. & Gill, D. M. (1989). *EMBO J.* **8**, 1087–1092.
Evans, H. R., Sutton, J. M., Holloway, D. E., Ayriss, J. A., Shone, C. C. & Acharya, K. R. (2003). *J. Biol. Chem.* **278**, 45924–45930.
French, S. & Wilson, K. (1978). *Acta Cryst.* A**34**, 517–525.
Habermann, B., Mohr, C., Just, I. & Aktories, K. (1991). *Biochem. Biophys. Acta*, **1077**, 253–258.
Han, S., Arvai, A. S., Clancy, S. B. & Tainer, J. A. (2001). *J. Mol. Biol.* **305**, 95–107.
Jones, T. A., Zou, J. Y., Cowan, S. W. & Kjeldgaard, M. (1991). *Acta Cryst.* A**47**, 109–110.
Laskowski, R. A., MacArthur, M. W., Moss, D. S. & Thornton, J. M. (1993). *J. Appl. Cryst.* **26**, 283–291.
Lehmann, M., Fournier, A., Selles-Navarro, I., Dergham, P., Sebok, A., Leclerc, N., Tigyi, G. & McKerracher, L. (1999). *J. Neurosci.* **19**, 7537–7547.
Ménétrey, J., Flatau, G., Stura, E. A., Charbonnier, J.-B., Gas, F., Teulon, J.-M., Le Du, M.-H., Boquet, P. & Ménez, A. (2002). *J. Biol. Chem.* **277**, 30950–30957.
Murshudov, G. N., Vagin, A. A. & Dodson, E. J. (1997). *Acta Cryst.* D**53**, 240–255.
Otwinowski, Z. & Minor, W. (1997). *Methods Enzymol.* **276**, 307–326.
Perrakis, A., Morris, R. M. & Lamzin, V. S. (1999). *Nature Struct. Biol.* **6**, 458–463.
Rubin, E. J., Gill, D. M., Boquet, P. & Popoff, M. R. (1988). *Mol. Cell. Biol.* **8**, 418–426.
Vagin, A. & Teplyakov, A. (1997). *J. Appl. Cryst.* **30**, 1022–1025.
Watanabe, Y., Morimatsu, M. & Syuto, B. (2000). *J. Vet. Med. Sci.* **62**, 473–478.
Wilde, C. & Aktories, K. (2001). *Toxicon*, **39**, 1647–1660.
Wriggers, W. & Schulten, K. (1997). *Proteins*, **29**, 1–14.